Available online at www.sciencedirect.com
ScienceDirect
Journal of Solid State Chemistry 180 (2007) 158–166
JOURNAL OF SOLID STATE CHEMISTRY
www.elsevier.com/locate/jssc

Chemical twinning of the pyrochlore structure in the system Bi_2O_3–Fe_2O_3–Nb_2O_5

I.E. Grey[a,*], W.G. Mumme[a], T.A. Vanderah[b], R.S. Roth[b], C. Bougerol[c]

[a]*CSIRO Minerals, Box 312, Clayton South, Vic., 3169, Australia*
[b]*National Institute of Standards and Technology, Materials Science, and Engineering Laboratory, Gaithersburg, MD 20899, USA*
[c]*Equipe CEA-CNRS NPSC SP2M/DRFMC/CEA, 17 rue des Martyrs, 38054 Grenoble, France*

Received 18 July 2006; received in revised form 25 September 2006; accepted 1 October 2006
Available online 10 October 2006

Abstract

New ternary bismuth iron niobates having structures based on chemical twinning of pyrochlore are described. $Bi_{5.67}Nb_{10}FeO_{35}$ has hexagonal symmetry, $P6_3/mmc$, $a = 7.432(1)$ Å, $c = 31.881(2)$ Å, $Z = 2$ and $Bi_{9.3}Nb_{16.9}Fe_{1.1}O_{57.8}$ has rhombohedral symmetry, $R\text{-}3m$, $a = 7.433(1)$ Å, $c = 77.488(2)$ Å, $Z = 3$. The structures of both phases were determined and refined to $R_1 = 0.04$ using single-crystal X-ray data. They can be described as being derived from the pyrochlore structure by chemical twinning on $(111)_{py}$ oxygen planes. The chemical twin operation produces pairs of corner-connected hexagonal tungsten bronze (HTB) layers as in the HTB structure, so the structures may alternatively be described as pyrochlore:HTB unit-cell intergrowth structures. In the hexagonal phase the pyrochlore blocks have a width of 12 Å, whereas the rhombohedral phase has pyrochlore blocks of two widths, 6 and 12 Å, alternating with HTB blocks. It is proposed that the previously reported binary $4Bi_2O_3$:$9Nb_2O_5$ phase has a related structure containing pyrochlore blocks all of width 6 Å. A feature of the structures is partial occupancy (~65%) of the Bi sites and displacement of the Bi atoms from the ideal pyrochlore *A* sites towards the surrounding oxygen atoms, as observed in Bi-containing pyrochlores.

Keywords: Chemical twinning of pyrochlore; Pyrochlore:HTB unit-cell intergrowths

1. Introduction

In their 1962 phase equilibria study of the Bi_2O_3–Nb_2O_5 system, Roth and Waring [1] identified a new phase with composition $4Bi_2O_3$:$9Nb_2O_5$ that was stable only in a narrow temperature range, 1070–1183 °C. They were able to index the stronger reflections in the powder X-ray diffraction (XRD) pattern using a hexagonal cell with $a = 6.447$ Å, $c = 19.778$ Å. However a number of weaker reflections could not be indexed using this cell. The incongruent melting point and the narrow temperature range of stability of the 4:9 phase thwarted all attempts to grow single crystals, and its structure remained unknown.

A recent phase equilibria study of the ternary system Bi_2O_3–Fe_2O_3–Nb_2O_5 [2] revealed the presence of two new ternary phases with powder XRD patterns related to that for the 4:9 binary phase. Analyses of single crystals of the two phases showed related hexagonal unit cells with a common *a* lattice parameter of 7.433(1) Å and with different *c* parameters of 31.881(2) and 77.488(2) Å. The symmetries were hexagonal and rhombohedral, respectively. The phase equilibria results obtained from the disappearing phase method, combined with electron microprobe analyses of the single crystals, indicated that the phases form at only slightly different stoichiometries, with Bi_2O_3:Fe_2O_3:Nb_2O_5 mole ratios of 34:6:60 for the hexagonal phase and 34:4:62 for the rhombohedral phase. The two compositions nearly lie on a straight line joining the 4:9 binary composition to a pyrochlore phase field in the middle of the ternary diagram [2] as illustrated in Fig. 1. The pyrochlore solid solution region is extended in the direction of the line towards the 4:9 phase and is relatively narrow normal to this line, suggesting that the two ternary phases and the 4:9 binary phase may be crystal-chemically related to pyrochlore. We describe here the structure

*Corresponding author. Fax: +61 3 9562 8919.
E-mail address: ian.grey@csiro.au (I.E. Grey).

0022-4596/$ - see front matter © 2006 Elsevier Inc. All rights reserved.
doi:10.1016/j.jssc.2006.10.004

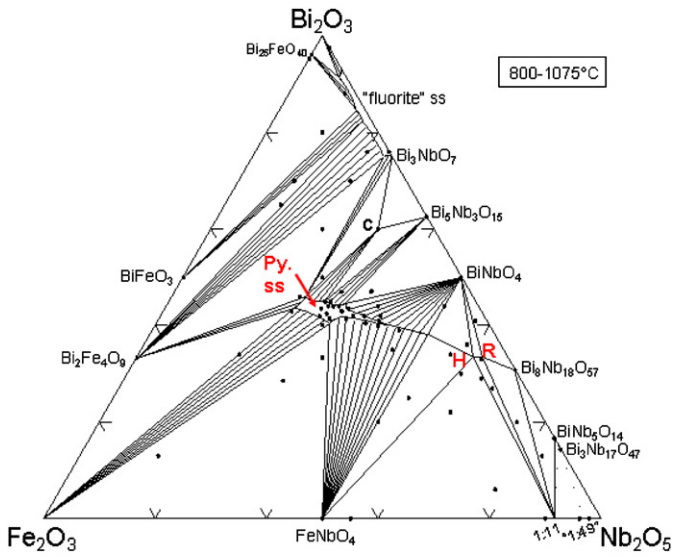

Fig. 1. Ternary Bi_2O_3–Fe_2O_3–Nb_2O_5 phase diagram showing location of the rhombohedral (R) and hexagonal (H) phases with Bi_2O_3:Fe_2O_3:Nb_2O_5 molar ratios of 34:4:62 and 34:6:60 respectively. The pyrochlore solid solution phase field is labelled Py. ss.

determinations for the two ternary phases, and their relationships with pyrochlore and the 4:9 structures.

2. Experimental

2.1. Syntheses

Single crystals of the two ternary phases were grown by slowly cooling off-stoichiometric melts of equilibrated powders [2], contained in platinum capsules sealed by welding. The samples were heated to 1300 °C and then cooled at 3 °C/h (rhombohedral phase crystals) or 5 °C/h (hexagonal phase crystals) to below the solidus (800–900 °C) followed by air quenching. Starting powders with Bi_2O_3:Fe_2O_3:Nb_2O_5 molar ratios of 35:3:62 and 33:5:62 yielded predominantly crystals of the rhombohedral and hexagonal phases, respectively, with minor amounts of the other phase. The crystals exhibited conchoidal fracture and were harvested as shards from the product mixtures. The rhombohedral phase crystals were distinguishable from the amber-colored hexagonal phase crystals by their lighter yellow color.

Crystals of the two phases were analysed using a JEOL[1] Superprobe operated in wavelength dispersive mode at 15 kV. Single crystals of $BiNbO_4$, $FeNbO_4$ and $Bi_2Fe_4O_9$ were used as standards. The molar compositions were obtained by averaging the results of 9 point analyses on different crystals of each phase.

[1]The use of brand or trade names does not imply endorsement of the product by NIST.

2.2. Single-crystal structural studies

The precession method was used for preliminary examination of the quality of the crystals and selection of suitable crystals for data collections. Crushed fragments of the crystals were also examined by transmission electron microscopy, using a JEOL 4000EX microscope with a spherical aberration coefficient of 1.06 mm. The microscope was operated at 400 kV. The samples were finely ground with ethanol in an agate mortar and pestle, and the suspension was transferred to a holey carbon grid for the study.

Single-crystal intensity data were collected at room temperature using a Bruker APEX II Kappa CCD diffractometer. The data collection and processing conditions are summarised in Table 1. The CCD intensity data sets were processed to produce absorption-corrected data files which were used with SHELXL [3] for the structure determinations and refinements.

Hexagonal 34:6:60 phase: The structure was solved using a Patterson synthesis to establish the positions of the Bi and Nb atoms. Their disposition corresponded to a *fcc* arrangement that was mirrored on $(111)_{fcc}$ planes (= (001) of the hexagonal cell) of oxygen atoms with a $0.5c$ repeat of 15.9 Å. Some difficulty was experienced at first with metal atom identification, because the Bi sites are only ~60% occupied, and so have similar scattering contrast to the Nb atoms. This gives rise to a pronounced $1/2a = 3.7$ Å subcell and only weak reflections corresponding to the full cell with $a = 7.4$ Å. A complete model, including oxygen positions, was developed on the basis that the *fcc* blocks corresponded to blocks of pyrochlore type. The atomic coordinates for the oxygen atoms were obtained from the published structure for the pyrochlore-related $Pb_2Nb_2O_7$ phase [4] which contains $(111)_{py}$ pyrochlore blocks. The Bi and Nb atoms were located in ideal pyrochlore positions. The general validity of the model was checked by generating a powder XRD pattern and confirming that it closely matched the experimental pattern for ground crystals.

Refinement of the model in $P6_3/mmc$ against the single crystal data resulted in poor convergence (R_1~20%). Difference Fourier syntheses showed clusters of strong peaks at the Bi positions, separated by only ~0.5 Å. The ideal-site Bi positions were progressively replaced by the split atomic positions, resulting in a marked improvement in the refinement. It was established that the oxygen atoms that bonded only to Bi (the O′ sites in oxide-pyrochlores, $A_2B_2O_6O'$) were also only partially occupied. The site occupancies of both the Bi and O′ sites were refined. The small amount of Fe present in the phase was distributed over the Nb sites. The final refinement, involving anisotropic displacement parameters of all atoms, converged at $R_1 = 0.040$ for 2411 reflections with $F > 4\sigma(F)$. Other refinement details are given in Table 1. The structural parameters from the refinement are reported in Table 2.

Table 1
Summary of data collection conditions and refinement parameters

Formula	$Bi_{9.3}Nb_{16.9}Fe_{1.1}O_{57.8}$	$Bi_{5.67}Nb_{10}FeO_{35}$
Crystal data		
Cell parameters	$a = 7.433(1)$ $c = 77.488(2)$ Å	$a = 7.432(1)$ $c = 31.881(2)$ Å
Z	3	2
Space group	$R\text{-}3m$	$P6_3/mmc$
Data collect		
Temperature (K)	300	300
λ (Mo$K\alpha$)	0.71073	0.71073
Crystal size	lath, $0.1 \times 0.1 \times 0.05$ mm	Triangular plate, 0.1 mm on edge, 0.05 mm thick
Collection mode	ϕ scan, 0–360°, $\Delta\phi = 0.5°$ plus ω scans	ϕ scan, 0–360°, $\Delta\phi = 0.5°$ plus ω scans
Count time per frame	60 s	30 s
$2\theta_{max}$ (deg)	70	101
Reflection range	$-12 \leqslant h,k \leqslant 12$; $-124 \leqslant l \leqslant 124$	$-16 \leqslant h,k \leqslant 6$; $-69 \leqslant l \leqslant 68$
Total no. reflections	47,909	143,634
Data completeness	95.7% at res. of 0.62 Å	94.6% at res. of 0.46 Å
No. unique reflections	2165	3163
No. reflections, $F > 4\sigma(F)$	1963	2411
Absorption correction	$\mu = 37.2\ mm^{-1}$	$\mu = 36.9\ mm^{-1}$
(Empirical—SADABS)	$T_{min}/T_{max} = 0.48$	$T_{min}/T_{max} = 0.52$
R_{merg} on F^2	0.048	0.075
Refinement		
No. parameters refined	138	103
R_1, $F > 4\sigma(F)$	0.041	0.040
R_1, all data	0.046	0.061
$wR_2(F^2)$[a], all data	0.091	0.115
GOF	1.20	0.79

[a] $w = 1/[\sigma^2(F_o^2) + (aP^2 + bP]$, $P = [2F_c^2 + \mathrm{Max}(F_o^2, 0)]/3$ from Ref. [3].

Table 2
Atomic coordinates ($\times 10^4$) and equivalent isotropic displacement parameters (Å$^2 \times 10^3$) for hexagonal $Bi_{5.67}Nb_{10}FeO_{35}$

Atom	Occup.	x	y	z	U(eq)
Nb(1)	0.91Nb/0.09Fe	3343(1)	1672(1)	3077(1)	12(1)
Nb(2)	0.91Nb/0.09Fe	6667	3333	4045(1)	12(1)
Nb(3)	0.91Nb/0.09Fe	0	5000	5000	11(1)
Bi(1A)	0.40(3)	3007(5)	6993(5)	3060(1)	22(1)
Bi(1B)	0.16(3)	3637(8)	7274(16)	3073(2)	13(3)
Bi(2A)	0.17(1)	2080(10)	3490(8)	4119(3)	22(1)
Bi(2B)	0.34(3)	2073(12)	3277(8)	4001(4)	19(1)
Bi(2C)	0.16(2)	1577(2)	3153(4)	3944(1)	16(2)
Bi(3)	0.624(4)	255(2)	509(5)	5005(5)	23(1)
O(1)	1.0	2637(6)	1318(3)	2500	12(1)
O(2)	1.0	5390(2)	780(5)	3016(1)	14(1)
O(3)	1.0	1256(2)	2512(5)	3233(1)	15(1)
O(4)	1.0	4073(4)	2037(2)	3712(1)	14(1)
O(5)	1.0	9208(4)	4604(2)	4401(1)	16(1)
O(6)	1.0	7940(2)	5880(5)	5125(1)	15(1)
O(7)	0.624(4)	3333	6667	3690(6)	51(4)
O(8)	0.624(4)	0	0	4240(6)	53(4)

U(eq) is defined as one third of the trace of the orthogonalized U^{ij} tensor.

Rhombohedral 34:4:62 phase: The structural principles established from the determination of the structure of the hexagonal phase were applied to solve the structure of the rhombohedral phase. The primitive cell c-axis repeat for the rhombohedral phase is $1/3c = 25.8$ Å $= 15.9$ Å $+ 9.9$ Å, where the first distance is the pyrochlore-block repeat in the hexagonal phase, and the second distance corresponds to a pyrochlore block with one less 6 Å-wide pyrochlore

Table 3
Atomic coordinates ($\times 10^4$) and equivalent isotropic displacement parameters (Å $\times 10^3$) for rhombohedral $Bi_{9.3}Nb_{16.9}Fe_{1.1}O_{57.8}$

Atom	Occup.	x	y	z	U(eq)
Nb(1)	0.94Nb/0.06Fe	3333	6666	7941(1)	12(1)
Nb(2)	0.94Nb/0.06Fe	1667	8333	8333	12(1)
Nb(3)	0.94Nb/0.06Fe	8333	1667	9126(1)	13(1)
Nb(4)	0.94Nb/0.06Fe	8333	1667	9602(1)	13(1)
Nb(5)	0.94Nb/0.06Fe	0	0	0	13(1)
Bi(1A)	0.21(1)	3214(8)	2005(14)	7964(2)	22(1)
Bi(1B)	0.48(1)	3441(3)	2038(4)	7910(1)	20(1)
Bi(2)	0.648(6)	6105(9)	3052(4)	8335(3)	16(1)
Bi(3)	0.554(4)	2711(2)	6356(1)	9131(1)	32(1)
Bi(4)	0.615(4)	2753(2)	6377(1)	9597(1)	28(1)
Bi(5A)	0.29(4)	5087(5)	4913(5)	−43(2)	19(4)
Bi(5B)	0.46(4)	5472(15)	5472(15)	0	23(2)
O(1)	1.0	2016(3)	4031(7)	639(1)	12(1)
O(2)	1.0	1271(4)	2543(8)	9149(1)	16(1)
O(3)	1.0	810(7)	5405(4)	339(1)	15(1)
O(4)	1.0	4609(4)	9217(8)	8384(1)	16(1)
O(5)	1.0	2546(7)	1273(4)	426(1)	14(1)
O(6)	1.0	825(8)	5412(4)	940(1)	16(1)
O(7)	1.0	−1296(3)	1296(3)	8863(1)	14(1)
O(8)	1.0	2062(3)	7938(3)	8088(1)	16(1)
O(9)	1.0	1297(3)	2594(7)	140(1)	13(1)
O(10)	0.648(6)	0	0	5316(3)	50(3)
O(11)	0.615(4)	0	0	3206(3)	50(3)
O(12)	0.554(4)	0	0	2211(4)	50(3)

U(eq) is defined as one third of the trace of the orthogonalized U_{ij} tensor.

repeating unit. A model was constructed in R-3m based on mirroring of pyrochlore blocks of two different widths and its validity checked by generating a powder XRD pattern, which was found to be in good agreement with the experimental pattern when correct partial occupancy of the Bi sites was allowed for.

Refinement of the single crystal data required a similar splitting of the Bi sites as found for the hexagonal phase, and also for Bi-containing pyrochlore structures [2,5,6]. A similar refinement procedure was followed as for the hexagonal phase, with the minor Fe content distributed over the Nb sites. The final refinement, with anisotropic displacement parameters, and with refinement of the site occupancies of the Bi and O′ atoms, resulted in convergence at $R_1 = 0.041$ for 1963 reflections with $F > 4\sigma(F)$. Other refinement details are given in Table 1. The structural parameters from the refinement are reported in Table 3.

3. Crystal chemistry

3.1. Hexagonal phase with Bi_2O_3:Fe_2O_3:$Nb_2O_5 = 34:6:60$

A polyhedral representation of the hexagonal phase, viewed along [110], is shown in Fig. 2. The corner-connected Nb/Fe-centred octahedra have the B_2O_6 topology of pyrochlore, $A_2B_2O_6O'$. The Bi atoms, shown by the

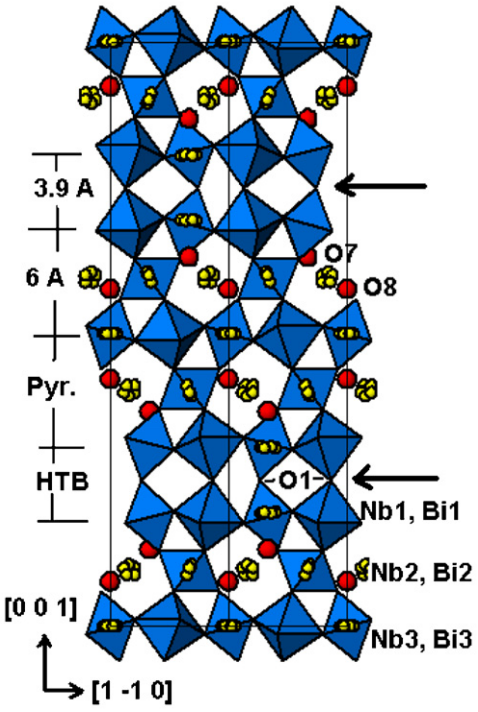

Fig. 2. Polyhedral representation of the hexagonal $Bi_{5.67}Nb_{10}FeO_{35}$ structure, viewed along [110]. Arrows show location of chemical twin planes. Bi atoms are shown as clusters of small circles. O′ atoms (O(7), O(8) are shown as larger circles.

small filled circles, occupy the A sites of pyrochlore, and are displaced from the ideal A site positions, forming clusters of partially occupied sites. The O′ atoms, O(7) and O(8) in Table 2, are co-ordinated only to Bi, and are shown by the larger circles in Fig. 2.

The A_2B_2 metal atom array of the stoichiometric pyrochlore structure forms a *fcc* lattice, with stacking of layers of two compositions, A_3B and B_3A along the four equivalent $\langle 111 \rangle_{py}$ directions. The B_3A layers comprise corner-linked BX_6 octahedra, forming the HTB motif. The A cations occupy the centres of the hexagonal rings of each of the four equivalent HTB layers. In hexagonal/rhombohedral pyrochlore-related structures, one of the four equivalent $\langle 111 \rangle_{py}$ directions becomes the hexagonal c-axis and the closest-packed A_3B and B_3A metal atom planes are then parallel to (001) of the hexagonal cell. The basic repeat unit of the hexagonal pyrochlore blocks is B_3A–A_3B–B_3A with a width of 6 Å. The pyrochlore blocks in the 34:6:60 hexagonal phase contain two such repeat units of total width = 12 Å as shown in Fig. 2.

Successive pyrochlore blocks are in a mirror relation. The mirror planes separating the pyrochlore blocks, at $z = \pm 0.25$, are shown with arrows in Fig. 2. They are located in the planes of the oxygen atoms shared between two B_3A layers, producing 2-layer-wide slabs of HTB-type structure of width 3.9 Å. The structure can thus be described as an intergrowth of HTB and pyrochlore blocks with a periodicity = 12 + 3.9 = 15.9 Å. The c-axis repeat of 31.8 Å contains two such sequences, related by the c glide operation of $P6_3/mmc$. Alternatively, considering the mirror-related pyrochlore blocks, the structure can be described as chemically twinned [7] pyrochlore.

If the Bi(1)–Bi(3) atoms occupied the ideal A sites of the pyrochlore blocks, they would be located at sites 4*f* (1/3,2/3,*z*) with $z = 0.3$, 12*k* (*x*,2*x*,*z*) with $x = 1/6$, $z = 0.4$ and 2*a* (0,0,1/2) respectively. The Bi atoms are displaced to more general sites in each case; Bi(1) to two different 12*k* sites, Bi(2) to two different 24*l* general positions and one 12*k* position, and Bi(3) to a 12*k* position. This results in 6 split sites for Bi(1) and Bi(3) and 5 split sites for Bi(2). The displacements of the Bi atoms from the ideal positions are in the range 0.22–0.47 Å.

The movement of the Bi atoms is towards each of the six oxygen atoms forming the hexagonal ring in the plane of the HTB layer in which the Bi atom is located. In the cases of Bi(1) and Bi(3) the HTB plane containing the Bi atoms is the (001) plane. As seen in Fig. 2 the six Bi atoms of the Bi(1) and Bi(3) clusters lie in the (001) plane. The environment of the Bi(3) atoms is viewed normal to (001) in Fig. 3. The displacement of the six partially occupied Bi sites is along the six $\langle 1\bar{1}0 \rangle$ directions, towards the six O(6) atoms forming the hexagonal ring of the HTB layer. The same type of planar cluster of six Bi sites, displaced towards the hexagonal-ring oxygen atoms, has been reported in Bi-containing pyrochlores [2,5,6].

In the case of Bi(2), there are only five displaced Bi sites. This can be understood in terms of the distances of the

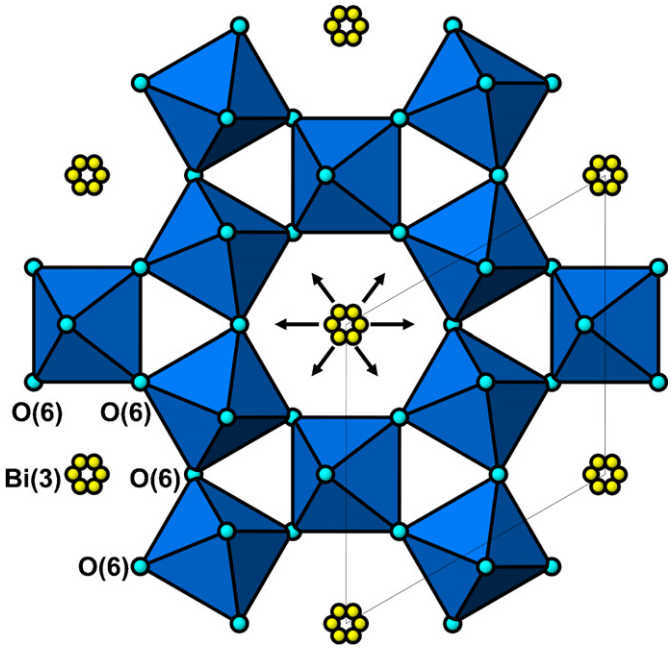

Fig. 3. (001) slice through the structure of hexagonal $Bi_{5.67}Nb_{10}FeO_{35}$ at $z = \frac{1}{2}$, showing splitting of Bi(3) site into six partially occupied sites, displaced towards O(6) of the HTB layer.

ideal (undisplaced) Bi to the surrounding six hexagonal-ring oxygen atoms. These are O(3), 2 × O(4), 2 × O(5) and O(6) at distances of 2.50, 2 × 2.59, 2 × 2.76 and 2.83 Å respectively. The "missing" displaced Bi is towards O(6). This involves the longest Bi–O distance and so satisfying the Bi valence requirements will be most difficult to achieve by displacement towards this oxygen atom.

By analogy with Bi-containing pyrochlores [2,5,6], the oxygen atoms O(7) and O(8), bonded only to Bi, should also be displaced from the ideal pyrochlore O′ sites. We obtained no clear indication of split O(7) and O(8) from the structure refinement, and the displacement parameters for these atoms are not strongly anisotropic. However the equivalent isotropic displacement parameters given in Table 2 are much higher than for the other oxygen atoms, suggestive of small displacements with an approximately spherical distribution.

The Bi–O and Nb–O distances are reported in Table 4, together with calculated bond valence sums [8]. The small amount of iron at the niobium sites was neglected in the bond valence calculations. The three niobium atoms have bond valence sums very close to 5. The bismuth atoms however are all under-saturated, with bond valence sums ranging from as low as 2.21 for Bi(3) to 2.79 for one of the split Bi(2) atoms. We also calculated bond valence sums for Bi atoms located at the *ideal* A site positions. This gave values of 2.52, 2.43 and 2.05 for Bi(1) to Bi(3), respectively. The displacement of the Bi atoms has in all cases led to an increase in the bond valence sum of typically 0.2 valence units. The low bond valence sum for the Bi(3) atom could be improved significantly by taking account of displacements of the O′ anions towards Bi(3) atoms. These atoms

Table 4
Bond lengths (Å) and bond valence sums (v.u.) for Bi and Nb in hexagonal $Bi_{5.67}Nb_{10}FeO_{35}$

M–O	Distance	*M*–O	Distance
Nb(1)–O(1)	1.894(1)	Nb(2)–O(4) × 3	1.978(3)
Nb(1)–O(2) × 2	1.949(2)	Nb(2)–O(5) × 3	1.991(3)
Nb(1)–O(3) × 2	2.003(2)	Nb(2) bond valence	4.92
Nb(1)–O(4)	2.079(2)		
Nb(1) bond valence	5.05	Nb(3)–O(5) × 2	1.977(2)
		Nb(3)–O(6) × 4	1.983(2)
		Nb(3) bond valence	4.97
Bi(1A)–O(7)	2.05(2)	Bi(2A)–O(7)	2.47(1)
Bi(1A)–O(3)	2.322(7)	Bi(2A)–O(6)	2.46(1)
Bi(1A)–O(2) × 2	2.469(4)	Bi(2A)–O(4)	2.58(1)
Bi(1A)–O(3) × 2	2.958(6)	Bi(2A)–O(5)	2.79(1)
Bi(1A)–O(2)	3.069(8)	Bi(2A)–O(3)	2.90(1)
Bi(1A) bond valence	2.66	Bi(2A)–O(4)	2.984(4)
		Bi(2A) bond valence	2.44
		Bi(2B)–O(8)	2.266(4)
Bi(1B)–O(7)	2.01(2)	Bi(2B)–O(4)	2.297(7)
Bi(1B)–O(2)	2.26(1)	Bi(2B)–O(7)	2.419(8)
Bi(1B)–O(3) × 2	2.552(5)	Bi(2B)–O(3)	2.52(1)
Bi(1B)–O(2) × 2	2.870(7)	Bi(2B)–O(5)	2.50(1)
Bi(1B)–O(3)	3.11(1)	Bi(2B)–O(4)	2.87(1)
Bi(1B) bond valence	2.79	Bi(2B)–O(6)	2.86(1)
		Bi(2B)–O(5)	3.038(4)
		Bi(2B) bond valence	2.60
Bi(3)–O(6)	2.361(6)	Bi(2C)–O(8)	2.239(8)
Bi(3)–O(8) × 2	2.44(2)	Bi(2C)–O(3)	2.301(4)
Bi(3)–O(6) × 2	2.533(5)	Bi(2C)–O(7)	2.402(7)
Bi(3)–O(6) × 2	2.859(5)	Bi(2C)–O(4) × 2	2.493(3)
Bi(3) bond valence	2.21	Bi(2C)–O(5) × 2	2.878(3)
		Bi(2C)–O(6)	3.034(5)
		Bi(2C) bond valence	2.68

have large equivalent isotropic displacement parameters, corresponding to mean-square displacements of ~0.2 Å. Such displacements of pairs of O(8) anions towards the Bi(3) atoms will increase the bond valence sums by up to 0.5 valence units.

The refined occupancies of the Bi sites are given in Table 2. Summing the site occupancies for the partially occupied Bi sites gives the following percent occupations: Bi(1) 56(4)%, Bi(2) 67(4)% and Bi(3) 62(4)%, with a weighted average occupation of 64%. Using the refined site occupancies for the Bi atoms and for the O′ atoms (O(7) and O(8)) the composition of the asymmetric unit is calculated to be $Bi_{5.76}Nb_{10}FeO_{35.50}$. This has an excess charge of −0.7. The small charge imbalance is well within the variation expected from the e.s.d. values on the refined Bi and oxygen site occupancies. For comparison the electron microprobe analyses, normalised to the $11 \times BO_3$ framework composition of $[Nb_{10}FeO_{33}]^{13-}$, gives a composition $Bi_{5.67}Nb_{10}FeO_{35.0}$, which is quite close to the composition determined from the site occupancy refinements, and is charge balanced. This formula is given in Table 1 as the formula for the hexagonal phase.

3.2. Rhombohedral phase with Bi_2O_3:Fe_2O_3:Nb_2O_5 = 34:4:62

A polyhedral representation of the structure of the rhombohedral phase, viewed along [110] is shown in Fig. 4. In contrast to the hexagonal phase in which the chemically twinned pyrochlore blocks all have the same thickness of 12 Å along [001], the structure of the rhombohedral phase contains pyrochlore blocks of two different widths, 6 and 12 Å. These are joined with pairs of HTB layers, separated by 3.9 Å, so the repeat along [001] for the asymmetric unit of the rhombohedral phase is 6 + 3.9 + 12 + 3.9 = 25.8 Å. Whereas in the hexagonal phase, the chemical twin planes are crystallographic mirror planes, in the rhombohedral phase this is not so; the Nb and Bi atoms on opposite sides of the twin planes are crystallographically independent.

As found for the hexagonal phase, the Bi atom sites in the rhombohedral phase are partially occupied and displaced from the ideal pyrochlore *A* site positions. The percent occupancies are 69(1), 65(1), 55(1), 61(1) and 75(6)% for sites Bi(1) to Bi(5), respectively, and the average Bi site occupancy is 67%. Taking the e.s.d.s of the refined site occupation factors into account, this is not significantly different from the 64% Bi site occupancy in the hexagonal phase. The magnitudes of the displacements of the individual Bi atoms from the ideal *A* sites are in a relatively narrow range of 0.29–0.40 Å. The directions of the displacements are towards the oxygen atoms forming the

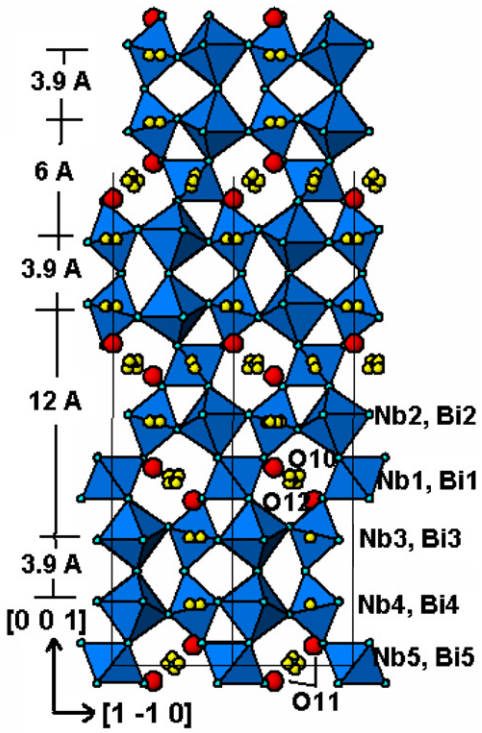

Fig. 4. Polyhedral representation of rhombohedral $Bi_{9.3}Nb_{16.9}Fe_{1.1}O_{57.8}$, viewed along [110]. The unit cell outline is shown from 0 to 1/3*c*. Bi atoms are represented by the small circles and O′ atoms (O(10), O(11) and O(12) by larger circles.

hexagonal ring around each Bi atom, as found for the hexagonal phase. However, the number of displaced Bi atoms is lower in the rhombohedral phase; Bi atoms in the Bi(3) and Bi(4) sites are displaced towards only three of the ring oxygens, and Bi(1) and Bi(5) are displaced towards four of the ring oxygens. Only Bi(2) located at a 2(a) site with symmetry $-3m$, is displaced towards all six ring oxygens.

The Nb–O and Bi–O distance ranges and calculated valence sums are reported in Table 5. The distances are comparable with those in the hexagonal phase. The Nb atoms in the HTB slabs, Nb(3) and Nb(4), have much wider bond length variations (ΔNb–O = 0.21 and 0.14 Å respectively) than the pyrochlore block Nb atoms (ΔNb–O = 0–0.01 Å). However the mean Nb–O distances are in a narrow range of 1.979–1.989 Å for all five Nb atoms and the bond valence sums at the Nb sites are all close to 5. The greatest deviation (valence sum 4.86 v.u.) is for the high symmetry Nb(5) site at the origin, suggesting that the minor iron component may be concentrated in this site. However there was no evidence of a lower-scattering element in this site from the displacement parameters, which are the same for all five Nb sites within one e.s.d.

The bond valence sums at the Bi sites are all low, as found also for the hexagonal phase. As previously discussed, the valence sums are very sensitive to the lengths of the short Bi–O′ bonds. This is well illustrated by the valence sums to Bi(3) and Bi(4) which are in similar environments in the HTB layers on either side of the chemical twin planes, see Fig. 4. The valence sum difference of 0.45 v.u. between the Bi(3) and Bi(4) sites is due predominantly to a 0.17 Å difference in the bond distances between these atoms and the O′ atoms, O(12) and O(11), respectively. The contribution to the bond valence sum from Bi(3)–O(12) at 2.006 Å is 1.26 v.u. while that from Bi(4)–O(11) at 2.173 Å is 0.81 v.u.

Table 5
Nb–O and Bi–O distance ranges (Å) and bond valence sums (v.u.) in rhombohedral $Bi_{9.3}Nb_{16.9}Fe_{1.1}O_{57.8}$

Nb atoms		Bi atoms	
Nb(1)–O range	1.978–1.993	Bi(1A)–O range	2.281–2.994
Nb(1)–O mean	1.985	Bi(1A) valence sum	2.45
Nb(1) valence sum	4.91		
		Bi(1B)–O range	2.248–3.016
Nb(2)–O range	1.972–1.984	Bi(1B) valence sum	2.63
Nb(2)–O mean	1.980		
Nb(2) valence sum	4.98	Bi(2)–O range	2.321–2.878
		Bi(2) valence sum	2.13
Nb(3)–O range	1.882–2.091		
Nb(3)–O mean	1.980	Bi(3)–O range	2.007–3.059
Nb(3) valence sum	5.06	Bi(3) valence sum	2.74
Nb(4)–O range	1.916–2.059	Bi(4)–O range	2.173–3.030
Nb(4)–O mean	1.979	Bi(4) valence sum	2.29
Nb(4) valence sum	5.03		
		Bi(5A)–O range	2.332–3.016
Nb(5)–O range	1.989 × 6	Bi(5A) valence sum	2.42
Nb(5)–O mean	1.989		
Nb(5) valence sum	4.86	Bi(5B)–O range	2.386–2.958
		Bi(5B) valence sum	2.48

An interesting feature common to both the hexagonal and rhombohedral structures is the absence of a second O′ atom coordinating to the Bi atoms in the HTB blocks. In pyrochlore, each A atom is coordinated to a pair of O′ atoms, on either side of the hexagonal ring in which it sits. Each O′ atom is surrounded by a tetrahedron of A atoms, giving the stoichiometry A_2O'. This stoichiometry is respected for the pyrochlore-block Bi atoms in the hexagonal and rhombohedral structures, but the Bi atoms in the HTB layers on either side of the chemical twin planes are coordinated to only one O′ atom.

From the refined site occupancies of the Bi and O′ atoms, the composition of the asymmetric unit of the rhombohedral phase is $Bi_{9.36}Nb_{16.91}Fe_{1.09}O_{57.6}$. The ratio of Fe to Nb comes from the microprobe analyses. The formula corresponds to a small charge imbalance of +0.8. The composition obtained from the microprobe analyses for Bi, Nb and Fe, normalised to 18 BO_3 units, is $Bi_{9.27}Nb_{16.91}Fe_{1.09}O_{57.81}$ which is charge balanced and matches closely with the results obtained using the Bi and O′ atom refined site occupancies. The latter composition, rounded to one decimal, is given in Table 1 as the formula for the rhombohedral phase.

The bismuth iron niobate intergrowth structures both have ~2/3 Bi: 1/3 vacancies in the A atom sites. Such a ratio might be expected to be conducive to short-range order of the filled and empty Bi sites. To investigate this possibility, a TEM study of crystals of the two ternary phases was conducted. Normally, electron diffraction (ED) patterns are sensitive indicators of short-range order of different atoms, or atoms and vacancies, and manifest the local order in the form of diffuse scattering. ED patterns were taken of many different zones, both including the c-axis and normal to the c-axis, but no evidence was found of concentrations of diffuse intensity.

[110] zone TEM images of the rhombohedral and hexagonal phases are shown in Figs. 5(a) and (b), respectively. In Fig. 5(a) the crystal thickness and defocus conditions result in the projected low charge density regions at the chemical twin planes appearing as white spots. The two different chemical twin plane separations of 9.9 and 15.9 Å for the rhombohedral phase are shown. In Fig. 5(b) the white spots correspond to projected columns of high charge density (Nb and Bi atoms) in the hexagonal phase. A simulated image, based on the structural parameters in Table 2, is shown in the centre of the experimental image in Fig. 5(b). TEM images such as those shown in Fig. 5 consistently showed that the phases were well ordered and free of mistakes in the intergrowth sequences.

4. Discussion

The two ternary Bi_2O_3–Fe_2O_3–Nb_2O_5 phases can be described either in terms of chemically twinned pyrochlore

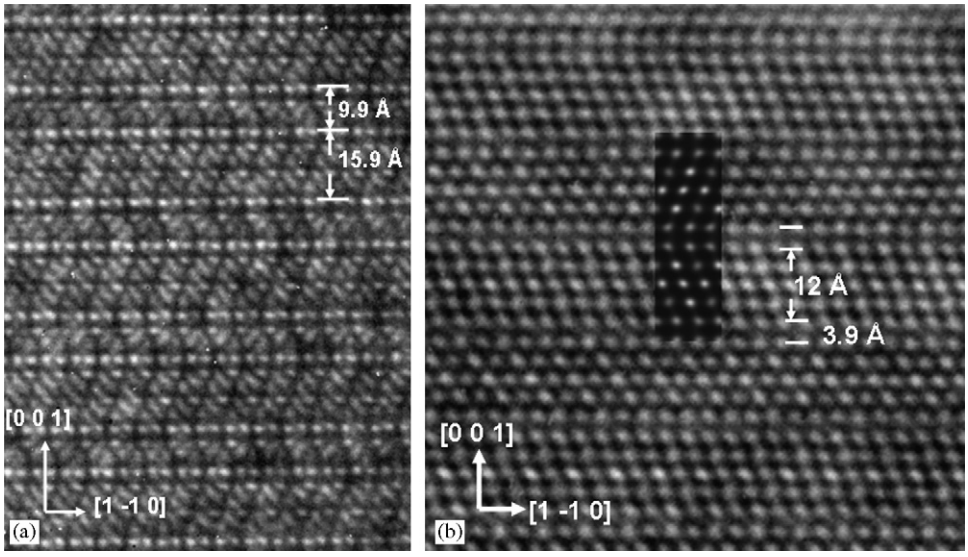

Fig. 5. [110] zone TEM images of (a) rhombohedral $Bi_{9.3}Nb_{16.9}Fe_{1.1}O_{57.8}$, and (b) hexagonal $Bi_{5.67}Nb_{10}FeO_{35}$. In (a) the sharp white spots correspond to empty sites along the chemical twin planes. In (b) the white spots correspond to Bi/Nb atoms. A simulated image is shown in the centre of Fig. 5(b).

or as unit-cell intergrowths of pyrochlore and HTB structures, parallel to $(111)_{py}\equiv(001)$ HTB. In the hexagonal phase the pyrochlore blocks have a fixed width of 12 Å, which as discussed in Section 3.1, corresponds to two repeat units of the pyrochlore structure normal to $(111)_{py}$. A shorthand notation for the pyrochlore:HTB intergrowth sequence in the hexagonal phase is 2:1. The rhombohedral phase contains pyrochlore blocks of two different widths, 6 and 12 Å. Using the shorthand notation the sequence of pyrochlore and HTB blocks is 2:1:1:1. The rhombohedral phase can thus be considered as an ordered intergrowth of the hexagonal-phase structure with a structure containing only 6 Å wide pyrochlore blocks. Such a structure would have hexagonal symmetry and a c-axis repeat which is a multiple of $6+3.9=9.9$ Å. As mentioned in the Introduction, the binary 4:9 Bi_2O_3:Nb_2O_5 phase has hexagonal symmetry with $c=19.778\,\text{Å}\approx 2\times 9.9\,\text{Å}$. To test if the 4:9 phase was the other end member of the intergrowth phases, a model was constructed in $P6_3/mmc$, using the coordinates of the 9.9 Å section of the rhombohedral phase appropriately scaled to the correct c-axis. The Rietveld-calculated pattern is compared with the experimental powder XRD pattern for the 4:9 phase in Fig. 6. The close match, even without refinement of the structure parameters, is consistent with the 4:9 phase having a structure based on the same structural principles as the ternary phases, thus representing the 1:1 pyrochlore:HTB intergrowth end-member.

The compositions of the intergrowth phases can be defined from the structural models. The composition of the octahedral frameworks in both HTB and pyrochlore is BO_3, and the topology of both structures is maintained in the intergrowth phases. Thus the framework composition in the intergrowth phases is also BO_3. The number, n, of BO_3 units per asymmetric cell is 7 for the 1:1 hexagonal phase and 11 for the 2:1 hexagonal phase. The number of A cations is $n-2$. Taking account of the observed fact that the A cations in the HTB blocks are bonded to only one O′ anion, the number of O′ atoms is $2\times 1/4+(n-4)\times 1/2=(n-3)/2$. The overall ideal formulae (no A site vacancies) is then $A_{n-2}B_nO_{3n}O'_{(n-3)/2}$. This expression gives the general structural formulae $A_5B_7O_{21}O'_2$ for the 1:1 hexagonal phase and $A_9B_{11}O_{33}O'_4$ for the 2:1 hexagonal phase. For the 2:1:1:1 rhombohedral intergrowth phase the ideal asymmetric unit formula (no A site vacancies) is obtained by adding the above two formulae, giving $A_{14}B_{18}O_{54}O'_6$. In the bismuth iron niobates described here, where $B=$ predominantly Nb, the above ideal structural formulae have a large excess of positive charge. Charge balance is achieved by partial occupancy of the A sites (Bi), with a corresponding reduction in occupancy of the O′ sites, giving the non-integral formulae reported in Table 1.

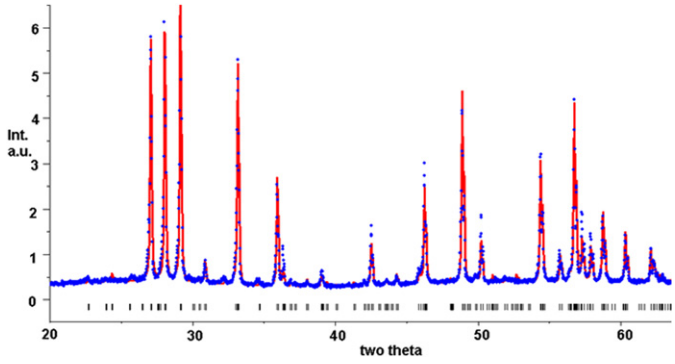

Fig. 6. Calculated (solid line) and experimental (dots) XRD pattern for 4:9 Bi_2O_3:Nb_2O_5, Cu$K\alpha$ radiation. The positions of the Bragg reflections are shown by the tick marks below the pattern.

Chemical twinning of pyrochlore on $(111)_{py}$ planes has been previously proposed to describe the TEM features of oxides in the systems Rb_2O–M_2O_5, $M=$ Ta, Nb and K_2O–Ta_2O_5 with compositions near 1:3 [9]. Hexagonal

phases designated as 9L and 16L were both proposed to contain the 9.9 Å structural blocks obtained by chemical twinning of 6 Å wide pyrochlore blocks. However, the chemically twinned blocks were further intergrown along the *c*-axis with blocks containing pairs of "fused" HTB layers containing edge-shared octahedra, so a simple description based on a single type of operation (chemical twinning) was not possible as it is for the phases described here.

We have recently described the determination of the structures of secondary hydrated tungsten oxides [10] that are closely related to the structures of the bismuth iron niobates described here. Pittongite, a new secondary tungsten mineral with simplified composition $Na_{0.22}[(W, Fe^{3+})(O,OH)_3]\cdot 0.44H_2O$ is hexagonal with $a = 7.286$ Å, $c = 50.49$ Å [10]. Using the above notation, the pyrochlore:HTB intergrowth sequence determined for pittongite is 2:1:2:1:1:1:1:1. It thus has double repeats of the 2:1 and 1:1 end-member sequences. However, the intergrowth sequence was not well developed in the low-temperature secondary mineral and TEM images showed that variations in the intergrowth sequence were common. The previously reported secondary tungstate mineral phyllotungstite [11] has a *c*-axis repeat of 19.55 Å and most likely has a structure based on chemical twinning of 6 Å wide pyrochlore blocks [10].

In further studies on the intergrowth phases we have prepared a large single-phase powder sample of the 4:9 *binary* phase for a neutron diffraction study to confirm the proposed model. Attempts to grow crystals of this phase are also in progress.

Acknowledgments

We thank Pierre Bordet, CNRS, Grenoble for collecting preliminary single crystal data sets that were used to determine the structures, Craig Forsyth, Monash University Chemistry Department, Melbourne, for collecting the single crystal data sets used for the refinements, and Mike Lufaso for assistance in identifying the ternary phases from powder XRD patterns.

References

[1] R.S. Roth, J.L. Waring, J. Res. Natl. Bureau Stand. A. Phys. Chem. 66A (6) (1962) 451–463.
[2] M.W. Lufaso, T.A. Vanderah, I.M. Pazos, I. Levin, R.S. Roth, J.C. Nino, V. Provenzano, P.K. Schenk, J. Solid State Chem. 179 (2006) 3900–3910.
[3] G.M. Sheldrick, SHELXL, University of Gottingen, Germany, 1997.
[4] H. Bernotat-Wulf, W. Hoffmann, Z. Kristallogr. 158 (1982) 101–117.
[5] I. Levin, T.G. Amos, J.C. Nino, T.A. Vanderah, C.A. Randall, M.T. Lanagan, J. Solid State Chem. 168 (2002) 69–75.
[6] T.A. Vanderah, I. Levin, M.W. Lufaso, Eur. J. Inorg. Chem. (2005) 2895–2901.
[7] S. Andersson, B.G. Hyde, J. Solid State Chem. 9 (1974) 92–101.
[8] N.E. Brese, M. O'Keeffe, Acta Crystallogr. B 47 (1991) 192–197 with updated R_o parameters from 〈http://www.ccp14.ac.uk/ccp/web-mirrors/i_d_brown/〉.
[9] K. Yagi, R.S. Roth, Acta Crystallogr. A 34 (1978) 765–773.
[10] I.E. Grey, W.D. Birch, C. Bougerol, S.J. Mills, J. Solid State Chem. 179 (2006) 3860–3869.
[11] K. Walenta, N. Jb. Miner. Mh. 12 (1984) 529–535.